J. Electroanal. Chem., 258 (1989) 243–264
Elsevier Sequoia S.A., Lausanne – Printed in The Netherlands

A new approach to electrochemical simulations based on eigenvector–eigenvalue solutions of the diffusion equations

Part I. Potentiostatic boundary conditions

Mark S. Friedrichs, Richard A. Friesner and Allen J. Bard

Department of Chemistry, The University of Texas at Austin, Austin, TX 78712 (U.S.A.)

(Received 4 January 1988; in revised form 19 September 1988)

ABSTRACT

An alternative approach to the digital simulation of electrochemical systems based on an eigenvector–eigenvalue analysis of the linear diffusion equations is presented. This approach is made feasible by recent innovations in the Lanczos algorithm and the development of the recursive generation residue method. We demonstrate that reductions in computation time of one to two orders of magnitude over explicit simulation techniques are possible with this technique for arbitrary, linear problems with a fixed-electrode potential; these gains are achieved without a loss in the flexibility and convenience in formulating and coding problems characteristic of time-stepping schemes.

(I) INTRODUCTION

Digital simulations have been widely employed in the solution of electrochemical problems, especially those involving complicated electrode geometries, applied potential functions (e.g., in cyclic voltammetry) or kinetic schemes [1,2]. Because explicit time-stepping methods are straightforward to formulate and code, even for irregular geometries, chemical kinetics, and boundary conditions, they have been very important in the development of electrochemical methodology and its application to the elucidation of chemical problems. However, the computation times are sometimes excessive even for systems of moderate size. For example, when the rate constants of coupled, homogeneous reactions are very large or the electrode geometries are such that two-dimensional diffusional effects must be treated, the finite difference schemes become computationally expensive since very small time increments must be employed. This liability, in addition to the desire to utilize microcomputers (rather than main frames) to carry out electrochemical simulations, has

0022-0728/89/$03.50

led to a search for more efficient numerical methods. Thus, exponentially expanding space [3,4] and time [4] grids, orthogonal collocation [5] and hop-scotch methods [6] have all been introduced in an effort to minimize the CPU time. The reductions, however, are often achieved at the expense of decreased flexibility and increased programming effort. For instance, with collocation techniques the program must be modified significantly when the kinetic scheme changes, and hence the method is in practice frequently inconvenient.

We present here a new approach to electrochemical simulations based on an eigenvector–eigenvalue analysis of the diffusion-kinetic equations (analogous to the treatment often employed in quantum mechanical problems). In this approach, the spatial variables in the diffusion-kinetic equations are discretized as in finite difference schemes; however, instead of also discretizing the time and then propagating the concentrations forward from the initial concentration profile, a system of decoupled equations is derived by decomposing the diffusion operator into its eigenmodes. The decoupled equations are then solved trivially to yield the flux at the electrode surface and hence the current. Note that in this approach the time variable is treated continuously, as opposed to conventional explicit algorithms in which time is discretized.

This strategy for solving a system of linear differential equations has been used for many years for relatively small systems and can be found in standard undergraduate linear algebra [7] and elementary differential equations [8] texts; nevertheless, it has not been applied to large systems (number of volume elements $\geqslant 500$) until recently due to the prohibitive computational times required by the available diagonalization algorithms. However, with the innovations by Paige [9,10], Cullum and Willoughby [11,12] and others in the Lanczos procedure and the subsequent development by Nauts and Wyatt [14,15] of the recursive residue generation method (RRGM), an eigenvector–eigenvalue analysis is now not only viable for large systems, but often qualitatively superior in terms of computational cost and convenience to alternative methods.

In this paper, we consider the simplest possible situation at the electrode; a fixed electrode potential with no coupled, homogeneous reactions. The mathematical details are set forth in the four subsections of Sect. (II). In the first, the matrix formulation of the diffusion operator, boundary conditions and flux operator is presented; Section (II.2) is devoted to a description of the eigenvector–eigenvalue analysis of the resulting system of equations and its physical interpretation. The third part focuses on the Green's function formalism in which the RRGM is couched, and Sect. (II.4) provides a brief outline of the Lanczos algorithm and RRGM; this subsection is elaborated on in Appendix A. Throughout the section, the Cottrell problem [2] is utilized to clarify the formalism and illuminate the somewhat abstract and perhaps unfamiliar mathematical constructs. In Sect. (III) results obtained for a two-dimensional model of a single microband electrode [16] using a finite difference scheme and an eigenvalue–eigenvector analysis based on the Lanczos algorithm and RRGM are presented; as discussed there, utilization of the latter technique reduces the CPU time of the explicit simulation by a factor of

30. A summary of the advantages of the approach introduced here is given in Sect. (IV).

We wish to stress at the outset that although the formalism in which the method is presented is complex and non-intuitive, and the details of its implementation rather involved, the actual computer program requires a minimal amount of programming effort on the part of the user, once the Lanczos method and RRGM have been coded. The primary user-supplied inputs are the initial concentration profile and flux operator cast in vector notation and a subroutine (completely analogous to the time-stepping portion of finite difference schemes) which calculates the concentration profile resulting from the application of the diffusion operator to a given profile. *Any formulation* of the diffusion operator, boundary conditions, and chemical kinetics can be used, as long as the resulting equations are *linear* in all concentrations. A single parameter, similar to the time step in an explicit program, is adjusted to fix the accuracy of the results.

In a forthcoming paper (Part II [17]), we will address problems in which an arbitrary time-dependent process occurs at the electrode surface (e.g., the linear sweep problem). For this class of problems, we obtain a surprising result: for a given geometry and set of bulk diffusive and reactive parameters, only one mass-transfer simulation needs to be performed. The current can then be obtained for *any* set of electrode dynamics by, in the simplest situation, evaluating a set of one-dimensional integrals or, in the most complicated, by solving a time-dependent integral equation for the flux. In either case, the calculation can be performed in negligible CPU time with even a microcomputer.

(II) MATHEMATICAL METHODS

(II.1) Matrix formulation of finite difference solution to Fick's equation

In most electrochemical problems, the bulk diffusion is assumed to be governed by Fick's equation,

$$\frac{\partial C(x, t)}{\partial t} = D \nabla^2 C(x, t) \tag{1}$$

(or its variant appropriately modified for homogeneous kinetics) where $C(x, t)$ is the concentration at position x and time t and D is the diffusion coefficient. The standard approach to solving eqn. (1) is to generate a system of finite difference equations. For example, the equation for a one-dimensional system can be approximated as the set of coupled, linear, first-order differential equations,

$$\frac{\mathrm{d}C_i}{\mathrm{d}t} = \frac{D}{\Delta x^2}(C_{i-1} - 2C_i + C_{i+1}) \tag{2}$$

where the spatial variable x has been partitioned into N discrete elements of width Δx, and C_i is the concentration of the species of interest in volume element i ($1 \leqslant i \leqslant N$). In explicit simulations, it is usual to consider the time similarly broken into discrete units Δt and to define a dimensionless, simulation diffusion coefficient

$D_M = (D\,\Delta t)/(\Delta x^2)$. However, in the approach presented here the temporal variable remains continuous, and we define a dimensional constant $D' = D/\Delta x^2$.

In addition to eqn. (1), the definition of the problem also requires the specification of the boundary concentrations (C_0) and C_{N+1} for a one-dimensional problem) and the initial concentration profile $C(x,\ t=0)$. The boundary condition at the electrode surface is determined by the particular electrode process; for example, $C(0,\ t) = f(E)$, where $f(E)$ is some function of the electrode potential E. Semi-infinite boundary conditions are typically imposed at the remaining boundaries for simulations in which the average diffusion path length during the time monitored is small compared to the linear dimensions of the system. For instance, if the initial concentration distribution is uniform and equal to C^*, then $C(x,\ t)$ is required to equal C^* in the limit as x approaches the system's boundaries.

To illustrate the above ideas in a matrix formulation, we consider the Cottrell problem defined by eqn. (2), the uniform initial concentration profile $C(x,\ 0) = C^*$, and the boundary conditions $C(0,\ t) = C_0$ and $C(\infty,\ t) = C^*$ with C_0 and C^* constants. For convenience, we normalize the concentrations by C^*; thus defining $c_i = C_i/C^*$, eqn. (2) becomes

$$\frac{\mathrm{d}c_i}{\mathrm{d}t} = D'c_{i-1} - 2D'c_i + D'c_{i+1} \qquad i = 1, \ldots, N \tag{3}$$

If $\boldsymbol{c}$ is the column vector of length N containing the c_i, and $\boldsymbol{W}$ is the $N \times N$ transfer matrix whose elements are given by

$$[\boldsymbol{W}]_{ij} = \begin{cases} -2D' & \text{if } i = j,\ i \neq N \\ -D' & \text{if } i = j,\ i = N \\ D' & \text{if } |i-j| = 1 \\ 0 & \text{otherwise} \end{cases} \tag{4}$$

then the system can be written in matrix form as

$$\frac{\mathrm{d}\boldsymbol{c}}{\mathrm{d}t} = \boldsymbol{W}\boldsymbol{c} + D'\boldsymbol{s}_0 \tag{5a}$$

where $\boldsymbol{s}_0$ is the column vector respresenting a source term arising from the electrode boundary condition and hence contains c_0 as its first element with all other elements zero. The other boundary condition $c_{N+1} = 1$, or equivalently $[\mathrm{d}c_{N+1}/\mathrm{d}t] = 0$ and $c_{N+1} = 1$ (at $t = 0$), is incorporated in the definition of $\boldsymbol{W}$. In explicit terms eqn. (5a) is

$$\left(\frac{\mathrm{d}}{\mathrm{d}t}\right)\begin{bmatrix} c_1 \\ c_2 \\ \cdot \\ \cdot \\ c_N \end{bmatrix} = \begin{bmatrix} -2D' & D' & 0 & 0 & \cdot & \cdot & \cdot \\ D' & -2D' & D' & 0 & \cdot & \cdot & \cdot \\ 0 & D' & -2D' & D' & 0 & \cdot & \cdot \\ \cdot & \cdot & \cdot & \cdot & \cdot & \cdot & \cdot \\ \cdot & \cdot & \cdot & \cdot & \cdot & D' & -D' \end{bmatrix}\begin{bmatrix} c_1 \\ c_2 \\ \cdot \\ \cdot \\ c_N \end{bmatrix} + D'\begin{bmatrix} c_0 \\ 0 \\ \cdot \\ \cdot \\ 0 \end{bmatrix} \tag{5b}$$

Finally, we specify $\boldsymbol{c}(0)$ as the vector containing the initial concentration in each volume element; for the case under consideration, $\boldsymbol{c}(0)$ is therefore given by

$$\boldsymbol{c}(0) = \begin{bmatrix} 1 \\ 1 \\ \cdot \\ \cdot \\ 1 \end{bmatrix} \tag{6}$$

Calculation of the current requires an expression for the flux at the electrode surface, f, which is defined as

$$f = D\left(\frac{\partial C}{\partial x}\right)_{x=0} \tag{7}$$

For the Cottrell problem, the discrete representation of the flux is

$$f = \left(\frac{D}{\Delta x}\right)[c_1 - c_0] \tag{8}$$

Since the boundary concentration c_0 is known, only c_1 is needed to determine the flux. For an arbitrary geometry, e.g. a band electrode, eqn. (7) can be generalized to

$$f = \left(\frac{D}{\Delta x}\right)\left[\sum_j{}' \{c_j - s_j\}\right] \tag{9}$$

where the primed sum in eqn. (9) used to indicate the sum is restricted to cells adjacent to the electrodes, and the s_j are the components of $\boldsymbol{s}_0$. Equation (9) may be expressed more compactly by reverting to vector notation. Thus, defining $\boldsymbol{e}^{\mathrm{T}}$ to be the transpose of the vector with a one in the jth entry if cell j adjoins an electrode and 0 otherwise.

$$f = \left(\frac{D}{\Delta x}\right)[\boldsymbol{e}^{\mathrm{T}} \cdot \boldsymbol{c}(t) - \boldsymbol{e}^{\mathrm{T}} \cdot \boldsymbol{s}_0] \tag{10}$$

For the Cottrell problem,

$$\boldsymbol{e}^{\mathrm{T}} = [1 \quad 0 \quad 0 \quad \cdot \quad \cdot \quad 0] \tag{11}$$

Equations (8)–(10) are important because they show that the flux is proportional to the *sum* of the concentrations at the electrode surface, and therefore knowledge of the individual concentrations c_i is not necessary for the evaluation of f; this fact will be exploited in Sect. (II.3).

In summary, the electrochemical diffusion problem can be cast as a set of simultaneous linear ordinary differential equations (eqns. 3–5). The solution of these equations obtained from an eigenvalue–eigenvector analysis will lead, as shown below, to an expression for the electrode flux of the form $f = \Sigma_k a_k \exp[\lambda_k t]$. We later identify the λ_ks as the eigenvalues of $\boldsymbol{W}$ and the a_ks as the product of the projections of the corresponding eigenvectors onto the initial concentration profile and the flux vector (the residues). The remainder of the paper addresses an efficient approach to obtaining these sets of quantities.

(II.2) Eigenvalue–eigenvector analysis

A standard approach to solving a set of coupled, linear differential equations, such as eqns. (5), is to transform $\boldsymbol{W}$ into new a diagonal matrix [7,8], Λ. This diagonalization produces an equivalent representation of the system in which the transformed equations are decoupled and hence easily solved. The desired solutions in the original representation are then found by applying the inverse transformation.

Because the formulation of the Landzos algorithm used here is only valid for symmetric transfer matrices (although it can be generalized to unsymmetric forms [18,19]), we will assume in the remainder of this section that $\boldsymbol{W}$ is symmetric, i.e., $[\boldsymbol{W}]_{ij} = [\boldsymbol{W}]_{ji}$. For problems of physical interest where $\boldsymbol{W}$ is unsymmetric, a simple decomposition of $\boldsymbol{W}$ can often be effected so that the resulting matrix to be diagonalized is symmetric, and hence the techniques described in Sects. (II.3) and (II.4) below remain applicable (see Appendix B).

Assuming $\boldsymbol{W}$ is symmetric, a standard theorem from linear algebra states there exists a set of N linearly independent eigenvectors $\boldsymbol{y}_k$ of $\boldsymbol{W}$ and their associated eigenvalues λ_k such that

$$\boldsymbol{W}\boldsymbol{y}_k = \lambda_k \boldsymbol{y}_k \qquad k = 1, \ldots, N \tag{12a}$$

Furthermore, the eigenvectors are orthogonal, that is, the vector product $\boldsymbol{y}_k^{\mathrm{T}} \cdot \boldsymbol{y}_j = 0$ unless $k = j$. We define an eigenvector matrix $\boldsymbol{M}$ to contain in its kth column $\boldsymbol{y}_k$; its inverse, $\boldsymbol{M}^{-1}$, by the above orthogonality property is the transpose of $\boldsymbol{M}$ (the $\boldsymbol{y}_k$ are taken to be normalized to 1). Equation (12a) can therefore be written in matrix form as

$$\boldsymbol{W}\boldsymbol{M} = \boldsymbol{M}\Lambda \tag{12b}$$

where Λ is the diagonal matrix $[\Lambda]_{kk} = \lambda_k$.

The real-space representation of the system given by eqns. (5) is a set of coupled, first-order differential equations, i.e., the time derivative of c_1 depends on c_0 and c_2, the time derivative of c_2 depends on c_1 and c_3, etc.. These can be transformed into a decoupled representation by multiplying eqns. (5) by $\boldsymbol{M}^{-1}$. Accordingly,

$$\left(\frac{\mathrm{d}}{\mathrm{d}t}\right)(\boldsymbol{M}^{-1}\boldsymbol{c}) = \boldsymbol{M}^{-1}\boldsymbol{W}\boldsymbol{c} + \boldsymbol{D}'\boldsymbol{M}^{-1}\boldsymbol{s}_0 \tag{13}$$

Setting $\boldsymbol{x} = \boldsymbol{M}^{-1}\boldsymbol{c}$ and $\boldsymbol{z} = \boldsymbol{M}^{-1}\boldsymbol{s}_0$ and observing that $\boldsymbol{M}^{-1}\boldsymbol{W}\boldsymbol{c} = (\boldsymbol{M}^{-1}\boldsymbol{W})(\boldsymbol{M}\boldsymbol{M}^{-1}\boldsymbol{c})$ $= (\boldsymbol{M}^{-1}\boldsymbol{W}\boldsymbol{M})(\boldsymbol{M}^{-1}\boldsymbol{c}) = \boldsymbol{M}^{-1}\boldsymbol{W}\boldsymbol{M}\boldsymbol{x}$.

$$\begin{aligned}\left(\frac{\mathrm{d}\boldsymbol{x}}{\mathrm{d}t}\right) &= (\boldsymbol{M}^{-1}\boldsymbol{W}\boldsymbol{M})\boldsymbol{x} + \boldsymbol{D}'\boldsymbol{z} \\ &= \Lambda\boldsymbol{x} + \boldsymbol{D}'\boldsymbol{z}\end{aligned} \tag{14a}$$

where the last step follows from eqn. (12b). Explicitly, eqn. (14a) is

$$\left(\frac{\mathrm{d}}{\mathrm{d}t}\right)\begin{bmatrix} x_1 \\ x_2 \\ \cdot \\ \cdot \\ x_N \end{bmatrix} = \begin{bmatrix} \lambda_1 & 0 & 0 & \cdot & 0 \\ 0 & \lambda_2 & 0 & \cdot & 0 \\ \cdot & \cdot & \cdot & \cdot & \cdot \\ \cdot & \cdot & \cdot & \cdot & \cdot \\ 0 & 0 & \cdot & \cdot & \lambda_N \end{bmatrix}\begin{bmatrix} x_1 \\ x_2 \\ \cdot \\ \cdot \\ x_N \end{bmatrix} + \boldsymbol{D}'\begin{bmatrix} z_1 \\ z_2 \\ \cdot \\ \cdot \\ z_N \end{bmatrix} \tag{14b}$$

Because Λ is diagonal, the equations in eqns. (14a) and (14b) are no longer coupled, i.e.,

$$\left(\frac{dx_i}{dt}\right) = \lambda_j x_j + D' z_j \tag{14c}$$

and hence they may be immediately solved to yield

$$x_j(t) = \exp(\lambda_j t) x_j(0) + D'\left(\frac{z_j}{\lambda_j}\right)\left[\exp(\lambda_j t) - 1\right] \tag{15a}$$

or equivalently,

$$\boldsymbol{x}(t) = \exp(\Lambda t)\boldsymbol{x}(0) + D'\Lambda^{-1}\left[\exp(\Lambda t) - \boldsymbol{I}\right]\boldsymbol{z} \tag{15b}$$

where $\boldsymbol{x}(0) = \boldsymbol{M}^{-1}\boldsymbol{c}(0)$, $\boldsymbol{I}$ is the $N \times N$ identity matrix, and $\exp(\Lambda t)$ is the diagonal matrix with $[\exp(\Lambda t)]_{kk} = \exp(\lambda_k t)$. In the final step, eqns. (15) are multiplied by $\boldsymbol{M}$ to transform the solutions $\boldsymbol{x}(t)$ into the desired solutions $\boldsymbol{c}(t)$ in the real-space representation. In matrix notation, this gives

$$\boldsymbol{c}(t) = \boldsymbol{M}\left[\exp(\Lambda t)\boldsymbol{M}^{-1}\boldsymbol{c}(0) + D'\Lambda^{-1}\{\exp(\Lambda t) - \boldsymbol{I}\}\boldsymbol{M}^{-1}\boldsymbol{s}_0\right] \tag{16}$$

It should be noted that nowhere in the above derivation was the time variable discretized.

For relatively small systems, the standard approaches to finding the eigenvalues and eigenvectors of a matrix are based on the QR algorithm or one of its variants (e.g., the subroutine EIGRS from the IMSL library). Thus if $\boldsymbol{W}$ is supplied as an input, then $\boldsymbol{M}$ and Λ will be returned, whereupon $\boldsymbol{M}^{-1}$ can be obtained as the transpose of $\boldsymbol{M}$; equation (16) is then easily evaluated to yield the concentrations.

While this method is feasible for small systems and perhaps still competive with explicit schemes, it is inefficient for large problems in which the transfer matrix is sparse. Standard diagonalization algorithms such as the QR algorithm scale computationally as N^3 and require on the order of N^2 memory locations. In contrast, the procedure outlined below reduces both these requirements by a factor of N: the number of operations needed by the Lanczos algorithm grows as γN^2 and the storage as γN, where γ is the average number of non-zero entries per row in the transfer matrix. For the class of electrochemical problems considered here, γ is between 3 and 7 (depending on the dimension of the system), and consequently in these cases, the Lanczos procedure can provide a qualitative advantage over other eigenvalue routines.

In physical terms, the eigenvectors $\boldsymbol{y}_k$ are linear combinations of the concentrations; they constitute the static eigenmodes of the diffusion problem, while the λ_k govern the system's dynamics. The diffusion eigenmodes are analogous to the vibrational modes of a string or harmonic crystal, with the eigenvalues replacing the vibrational frequencies. Indeed, the only qualitative differences among the problems are the range of the eigenvalue spectra and the nature of the boundary conditions.

Given the structure of $\boldsymbol{W}$, the eigenvalues can be shown to be non-positive (Gerschgorin's theorem [7]); the λ_k therefore determine how quickly the eigenmodes

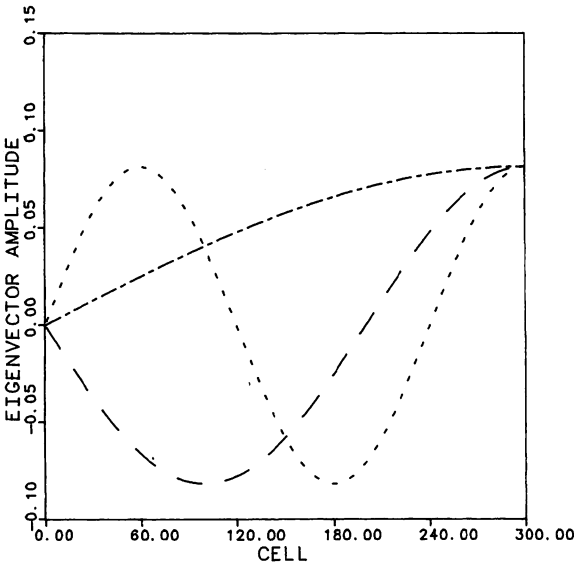

Fig. 1. The three eigenvectors (weighted linear combinations of the concentrations) of the Cottrell problem associated with the three eigenvalues smallest in absolute value: $\lambda_1 = -2.732 \times 10^{-5}$ (— - —), $\lambda_2 = -2.459 \times 10^{-4}$ (— —), and $\lambda_3 = -6.831 \times 10^{-4}$ (- - - - -).

relax to the their equilibrium value. Eigenvalues small in absolute value are generally correlated with long-wavelength eigenmodes, i.e., ones in which the variation of the eigenvector amplitudes between adjacent cells is small, whereas algebraically large eigenvalues are associated with eigenmodes of high spatial frequency. Because of the factors $\exp(\lambda_k t)$ multiplying the eigenvectors y_k in eqn. (16), the modes of high spatial frequency are quickly damped, so that only the long wavelength modes make a substantial contribution at long times. The physical basis for this is intuitively obvious: the diffusion process tends to smooth out any fluctuations in the concentration profile, and therefore in the absence of external forces, eigenmodes which vary rapidly are dissipated much earlier than those with a lower spatial frequency.

To illustrate these concepts, the concentrations in the Cottrell problem were evaluated by employing the IMSL subroutine EIGRS to calculate the eigenvalues and eigenvectors of the matrix $\boldsymbol{W}$ in eqn. (5b) with $D' = 1$, $\Delta x = 1$ and $N = 300$. The eigenvalues ranged in magnitude from -2.732×10^{-5} to -3.999. In Fig. 1 the normalized eigenvectors associated with the three eigenvalues smallest in absolute value are shown; in Figs. 2 and 3, the eigenvectors corresponding to the two eigenvalues largest in absolute value are exhibited. The plots are reminiscent of the vibrational modes of a string, with the curves in Fig. 1 corresponding to the fundamental and first two overtones, and Figs. 2 and 3 representing extremely high overtones. This observation is in accord with the earlier statement that eigenvectors

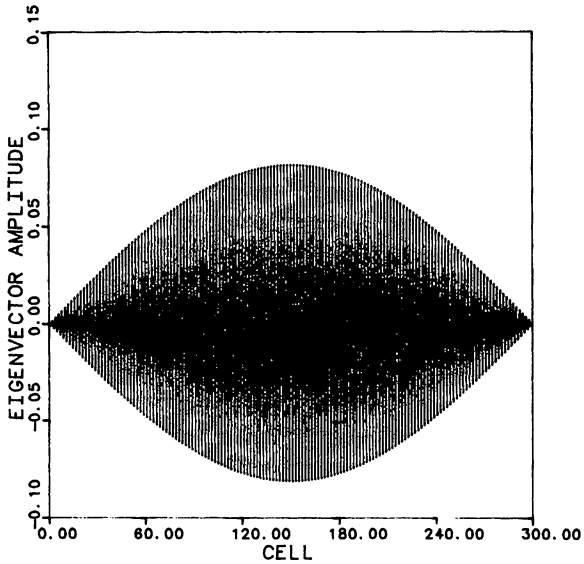

Fig. 2. Plot of the Cottrell eigenvector with the eigenvalue largest in magnitude, $\lambda_{300} = -3.9999$.

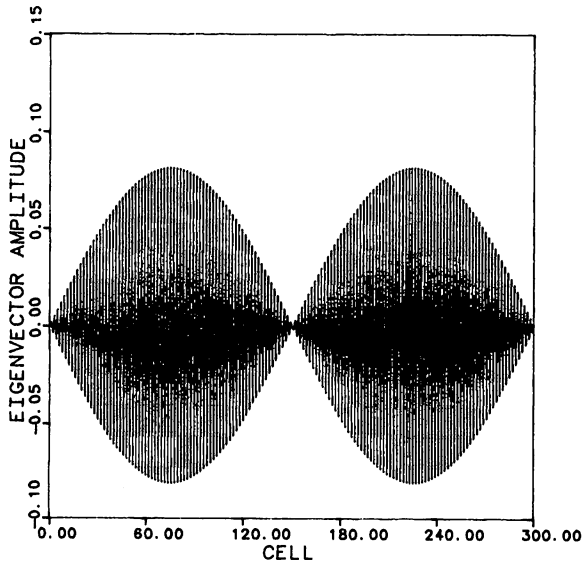

Fig. 3. Graph of the Cottrell eigenvector with the eigenvalue second largest in absolute value, $\lambda_{299} = -3.9996$.

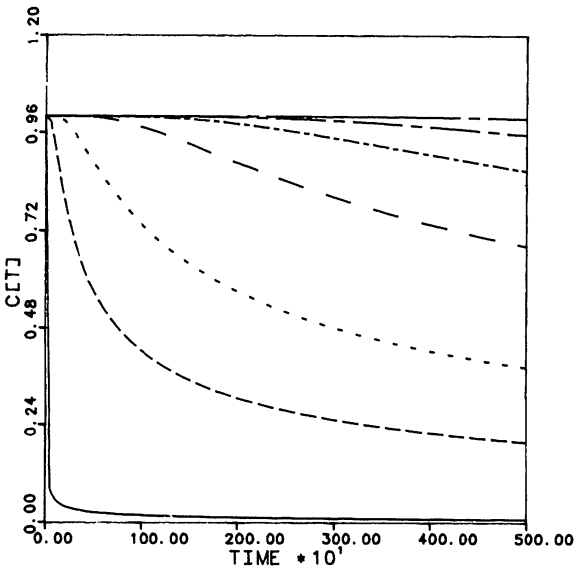

Fig. 4. The time dependence of the Cottrell concentrations at various positions in a system comprised of 300 cells. From top to bottom, the curves correspond to $c_{300}(t)$, $c_{200}(t)$, $c_{150}(t)$, $c_{100}(t)$, $c_{50}(t)$, $c_{25}(t)$, $c_{10}(t)$, and $c_1(t)$ where $c_i(t)$ is the concentration in cell i at time t, and the electrode is located at cell 0.

with eigenvalues small in absolute value vary slowly in comparison to those with eigenvalues at the other end of the spectrum.

Figure 4 is a graph of the concentrations at various locations in the system; these were derived using eqn. (16) with the initial concentration distribution $c_i(t=0)=1$ and the boundary concentrations $c_0=0$ and $c_{N+1}=1$. The bottommost curve, $c_1(t)$, is proportional to the flux since $c_0=0$; an analysis of its functional form shows it varies as $t^{-(1/2)}$, as predicted by analytical solutions for the current [2]. This is

TABLE 1

Comparison of the current calculated for the Cottrell problem using the numerical algorithm in the text with the analytic solution. The numerical results are obtained by taking $i(t)$ and dividing by $nFAD_0^{1/2}C_0^*$. The corresponding analytic quantity is $1/(\pi t)^{0.5}$

Time	Numerical	Analytic	Ratio
50	0.796×10^{-1}	0.797×10^{-1}	0.998
100	0.563×10^{-1}	0.564×10^{-1}	0.999
150	0.460×10^{-1}	0.460×10^{-1}	0.999
200	0.398×10^{-1}	0.398×10^{-1}	0.999
250	0.356×10^{-1}	0.356×10^{-1}	0.999
300	0.325×10^{-1}	0.325×10^{-1}	0.999
350	0.301×10^{-1}	0.301×10^{-1}	0.999
400	0.282×10^{-1}	0.282×10^{-1}	0.999
450	0.265×10^{-1}	0.265×10^{-1}	0.999
500	0.252×10^{-1}	0.252×10^{-1}	0.999

demonstrated explicitly in Table 1, where the flux computed via the present method is compared to the corresponding analytic solution. For all times, the difference between the two profiles is less than 1%.

The topmost curve, $c_{300}(t)$, demonstrates that in the time regime shown, the other boundary is unaffected by the electrode process. The intermediate concentrations display the time scale on which the electrode dynamics affect the various regions of the system and the distribution of the equilibrium concentrations.

For the remainder of this paper, we restrict our attention to the case $s_0 = 0$, i.e., the electrode potential is set so that $c_0 = 0$; the generalization represented by eqns. (5), however, presents no difficulties for the methods described subsequently.

(II.3) Green's function formalism

With s_0 set equal to zero, eqn. (16) becomes

$$\begin{aligned} \boldsymbol{c}(t) &= \boldsymbol{M} \exp(\Lambda t) \boldsymbol{M}^{-1} \boldsymbol{c}(0) \\ &= \exp[\boldsymbol{W}t]\boldsymbol{c}(0) \\ &= \boldsymbol{G}(t)\boldsymbol{c}(0) \end{aligned} \tag{17}$$

The matrix $\boldsymbol{G}(t) = \exp[\boldsymbol{W}t]$ is referred to as the Green's function operator; its matrix elements $G_{mn}(t)$ give the conditional probability that an ion initially in volume element n has diffused to cell m at time t. The matrix $\boldsymbol{G}(t)$ acting on the initial concentration vector therefore gives the concentration profile at time t.

In the vast majority of electrochemical experiments, the chief quantity of interest is the current, which is proportional to the total flux of the species being reduced at the electrode. From eqn. (10), the flux is in turn simply related to the concentration in the cells at the electrode surface. In the formalism of this section, eqn. (10) becomes ($s_0 = 0$)

$$\begin{aligned} f &= \left(\frac{D}{\Delta x}\right) \boldsymbol{e}^{\mathrm{T}} \cdot \boldsymbol{c}(t) \\ &= \left(\frac{D}{\Delta x}\right) \boldsymbol{e}^{\mathrm{T}} \cdot \boldsymbol{G}(t)\boldsymbol{c}(0) \\ &= \left(\frac{D}{\Delta x}\right) G_{ei}(t) \end{aligned} \tag{18}$$

The thrust of eqn. (18) is that $G_{ei}(t)$ is proportional to the flux to the electrode, and therefore is the primary information needed to analyze most experiments.

$G_{ei}(t)$ may be evaluated in terms of the eigenvalues and eigenvectors of $\boldsymbol{W}$. From eqn. (16) with $s_0 = 0$,

$$\begin{aligned} G_{ei}(t) &= \boldsymbol{e}^{\mathrm{T}} \cdot \boldsymbol{G}(t)\boldsymbol{c}(0) \\ &= \boldsymbol{e}^{\mathrm{T}} \cdot \{\boldsymbol{M} \exp[\Lambda t] \boldsymbol{M}^{-1}\} c(0) \\ &= \sum_{k=1}^{N} \boldsymbol{e}^{\mathrm{T}} \cdot \boldsymbol{y}_k \exp(\lambda_k t)\, \boldsymbol{y}_k^{\mathrm{T}} \cdot \boldsymbol{c}(0) \\ &= \sum_{k=1}^{N} R_{ei}^{(k)} \exp(\lambda_k t) \end{aligned} \tag{19}$$

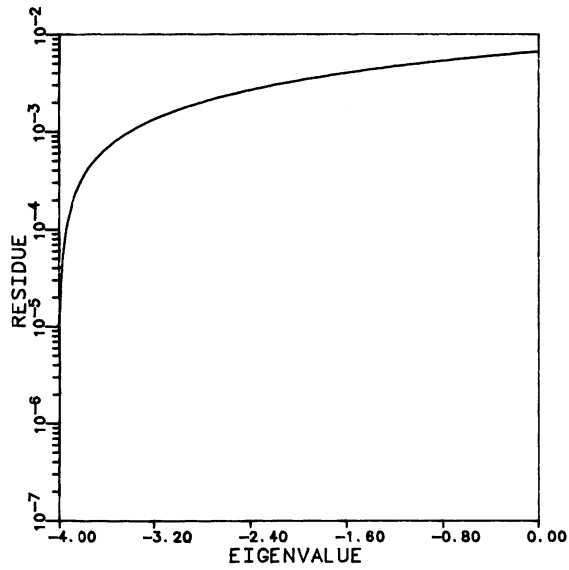

Fig. 5. Variation of the residues with respect to the associated eigenvalues for the Cottrell problem.

In the terminology of refs. 14 and 15, the products $R_{ei}^{(k)}$ are referred to as the residues of the system; they provide a direct measure of the coupling of the kth eigenmode to both the initial concentration distribution and the concentrations at the electrodes. Clearly, the residues associated with eigenvalues small in absolute value are important in determining the current's long-time behavior, while those residues with algebraically large eigenvalues contribute only to the transient response.

Figure 5 is a plot of the residues versus eigenvalues for the Cottrell problem. The residues are positive and decrease monotonically from a maximum of 6.655×10^{-3} for the eigenvalue smallest in absolute value to a minimum of 1.182×10^{-7} for the eigenvalue largest in absolute value. The primary source of the differences among the magnitudes of the residues is the factor $\boldsymbol{y}_k^{\mathrm{T}} \cdot \boldsymbol{c}(0)$. For the present problem, each entry of $\boldsymbol{c}(0)$ is one, and consequently the vector product $\boldsymbol{y}_k^{\mathrm{T}} \cdot \boldsymbol{c}(0)$ is simply the sum of the eigenvector amplitudes; this is tantamount to integrating the area under the sample curves shown in Figs. 1–3. Therefore due to the nearly complete cancellation of the areas above and below the abscissa, the total area for eigenvectors of high spatial frequency is much smaller than for eigenfectors of low frequency, thereby leading to smaller residues.

(II.4) The Lanczos algorithm and RRGM

The Lanczos algorithm and RRGM together constitute a numerical procedure for calculating the eigenvalues and residues of eqns. (19) which are strongly coupled to $\boldsymbol{e}$ and $\boldsymbol{c}(0)$. Both these quantities are found by using the Lanczos procedure to

generate a symmetric, tridiagonal matrix $\boldsymbol{T}$ which is related to $\boldsymbol{W}$ by a similarity transformation [7], i.e., $\boldsymbol{T} = \boldsymbol{V}^{-1}\boldsymbol{W}\boldsymbol{V}$, where $\boldsymbol{V}$ is the matrix of Lanczos vectors described in Appendix A. The important property of similarity transformations here is that the eigenvalues of the original and transformed matrix are identical. Because of $\boldsymbol{T}$'s simple and compact format (symmetric, tridiagonal), its eigenvalues and consequently $\boldsymbol{W}$'s may be determined efficiently using algorithms specifically designed for matrices of this form. $\boldsymbol{T}$ is also used to determine the residues via the RRGM formulated in refs. 14 and 15. By exploiting the structure of the Lanczos algorithm, the method allows the residues to be calculated with only the eigenvalues of $\boldsymbol{T}$ and $\boldsymbol{T}'$, the matrix obtained by deleting the first row and column of $\boldsymbol{T}$. The primary advantage of this approach is that the eigenvectors do not have to be determined explicitly thereby minimizing the time and storage required to calculate the observable.

In the remainder of this section, the similarities and differences between the procedure introduced here and explicit methods are noted briefly; a more detailed exposition of the Lanczos algorithm and the RRGM and their numerical implementation is provided in Appendix A.

The Lanczos algorithm is an iterative procedure involving various linear algebra manipulations, the most important of which is the operation of $\boldsymbol{W}$ on a vector. This multiplication is equivalent to the operation of $\boldsymbol{W}$ on $\boldsymbol{c}(t)$ to yield $\boldsymbol{c}(t + \Delta t)$ in finite difference schemes, and therefore any representation of the diffusion operator (including linear kinetic effects) used in explicit simulations may be employed. The only condition which must be satisfied in applying the scheme is that the resulting set of diffusion equations must be linear in the concentrations. Hence in contrast to other specialized techniques, the procedure described here retains the flexibility and ease of implementation characteristic of explicit methods.

Unlike the time-stepping procedures, however, the number of Lanczos iterations L depends not on the ratio of the final time to the time increment, but rather on the number of eigenmodes which are strongly coupled to the vectors $\boldsymbol{c}(0)$ and $\boldsymbol{e}$, and the accuracy to which the associated residues are required. The recursion number L plays the role of the time-step in explicit simulations: by increasing L (analogous to decreasing the time-step) more accurate solutions are obtained, and for L large enough convergence to the exact answer is secured. In practice L is typically only a fraction of the dimension of $\boldsymbol{W}$, and as a consequence the number of Lanczos recursions is substantially smaller than the number of iterations required in explicit schemes where numerical stability considerations require small time increments. Since the time for each Lanczos recursion is at most a small multiple of the time required for a finite difference time step, reductions of one to two orders of magnitude are possible.

(III) RESULTS

The flux for a single microband electrode was calculated using a finite difference scheme and the procedure outlined above. The model consisted of a two-dimen-

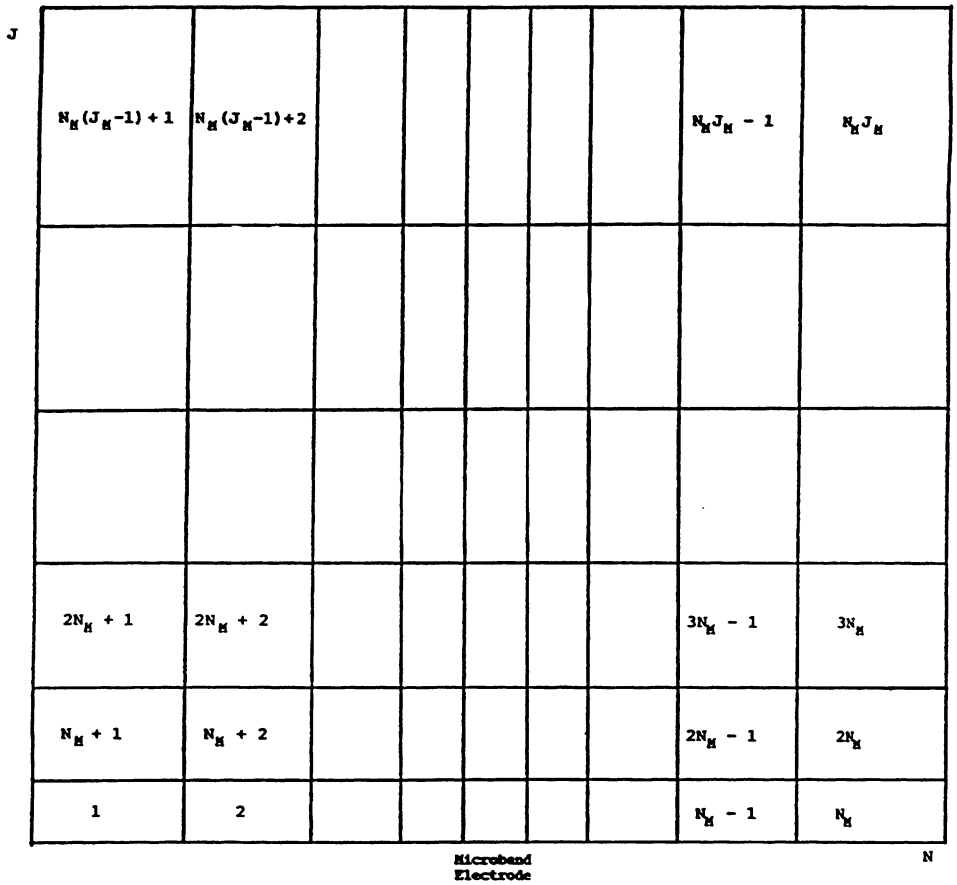

Fig. 6. Schematic of two-dimensional space grid used to model the microband electrode. The grid begins expanding exponentially to the left and right in the *N*-direction after the middle block of three uniform cells. The electrode is located at the center, bottommost cell. The grid also expands exponentially in the *J*-direction. The cells are labeled as indicated.

sional exponentially expanding space grid with the electrode lying in the plane of the substrate; a schematic of the grid configuration is presented in Fig. 6. Transport was assumed to be governed solely by diffusion (with no kinetics), and the initial bulk concentration distribution was taken to be uniform. In addition, the potential step of the model was set so that the concentration at the electrode goes instantaneously to zero; at the remaining edges, semi-infinite boundary conditions were imposed.

The exponential space grid in ref. 3 was utilized in order to reduce the computation time and extend the results to the long-time, quasi-steady-state regime. As shown in Appendix B, the employment of this type of grid renders the transfer matrix unsymmetric, and hence the procedure described above is not directly

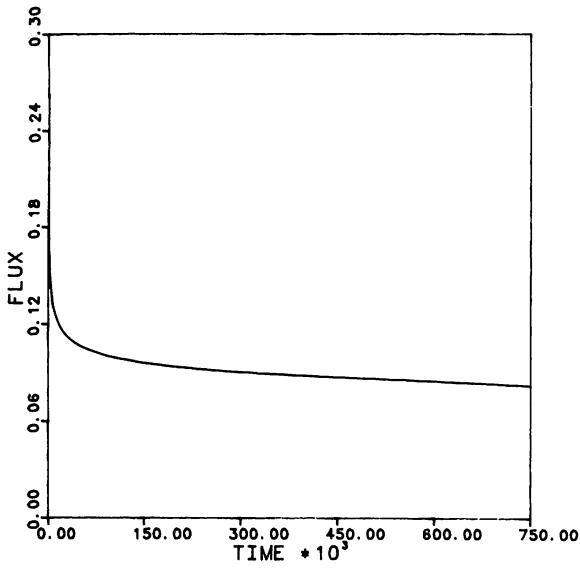

Fig. 7. Plot of the fluxes for a two-dimensional model of a single microelectrode (Fig. 6) which were calculated using an explicit simulation and the technique presented in the text.

applicable to $\boldsymbol{W}$. This problem can be circumvented, however, by factoring $\boldsymbol{W}$ into the form $\boldsymbol{U}^{-1}\boldsymbol{S}\boldsymbol{U}$, where $\boldsymbol{S}$ is symmetric and the structure of $\boldsymbol{U}$ is arbitrary, and then applying the RRGM to $\boldsymbol{S}$.

The resulting fluxes are shown in Fig. 7; they were obtained with $D_M = 0.24$ ($D' = D_M$ since Δt is set to 1) and were normalized by the initial concentration profile. Both calculations were performed on a Cray X-MP: the explicit simulation [16] required 97 CPU s (750,000 time steps), whereas the RRGM program took 3.2 s (1400 Lanczos iterations), an improvement by a factor of 30. The agreement between the two calculations is less than 0.1% at all times shown, and hence the two curves cannot be distinguished on the resolution of the plot. If a larger error is tolerable, reduction of the recursion number L and other adjustments could further enhance the RRGM's time.

Our computer code is presently designed so that the user need only supply the initial concentration and flux vectors and a subroutine to perform the matrix multiplication $\boldsymbol{W}\boldsymbol{q}$ (or $\boldsymbol{S}\boldsymbol{q}$ for the cases when $\boldsymbol{W}$ is unsymmetric) for an arbitrary vector $\boldsymbol{q}$; the program returns the electrode flux. We are presently in the process of generalizing the program so that it will handle arbitrary geometries and kinetic schemes automatically and still remain user-friendly.

(IV) CONCLUSION

In this paper, we have established the validity of the Lanczos algorithm and RRGM procedures for fixed-potential electrochemical simulations of arbitrary

geometry. It is apparent that our approach yields a greater timing improvement than most other sophisticated numerical methods (e.g., implicit time differencing, integral equations) without, for example, the associated constraints on the boundary conditions. This improvement should increase considerably the utility and convenience of digital simulations.

The limitation to fixed electrode potential is, however, rather restrictive. Consequently, Part II [17] is of great importance, since there this restriction will be removed completely. Indeed, the advance over conventional approaches achieved in the general case of non-trivial electrode kinetics is far greater than that demonstrated here, and should result in a qualitatively enhanced usage of simulation techniques.

APPENDIX A. THE LANCZOS ALGORITHM AND RRGM

In the following, we sketch the important details and formulas of the Lanczos procedure and RRGM and expand upon the discussion in Sect. (II.4). We concentrate here on the calculation of observables of the form $\boldsymbol{q}^{\mathrm{T}} \cdot \boldsymbol{G}(t)\boldsymbol{q} = G_{qq}(t)$, where $\boldsymbol{q}$ is an arbitrary vector. The evaluation of $\boldsymbol{q}^{\mathrm{T}} \cdot \boldsymbol{G}(t)\boldsymbol{q}'$, where $\boldsymbol{q}' \neq \boldsymbol{q}$ (for instance, $G_{ei}(t)$ in eqn. (19) with $\boldsymbol{q}^{\mathrm{T}} = \boldsymbol{e}^{\mathrm{T}}$ and $\boldsymbol{q}' = \boldsymbol{c}(0)$) can be reduced to this case by noting that

$$\begin{aligned}\boldsymbol{q}^{\mathrm{T}} \cdot \boldsymbol{G}(t)\boldsymbol{q}' &= \left(\tfrac{1}{2}\right)\left[\boldsymbol{a}^{\mathrm{T}} \cdot \boldsymbol{G}(t)\boldsymbol{a} - \boldsymbol{b}^{\mathrm{T}} \cdot \boldsymbol{G}(t)\boldsymbol{b}\right] \\ &= \left(\tfrac{1}{2}\right)\left[G_{aa}(t) - G_{bb}(t)\right] \end{aligned} \tag{A1}$$

where $\boldsymbol{a}$ is the vector $(1/\sqrt{2})(\boldsymbol{q} + \boldsymbol{q}')$ and $\boldsymbol{b} = (1/\sqrt{2})(\boldsymbol{q} - \boldsymbol{q}')$. Thus, two separate calculations of the procedure outlined below are required to determine $G_{ei}(t)$: $G_{aa}(t)$ and $G_{bb}(t)$ with $\boldsymbol{a} = (1/\sqrt{2})[\boldsymbol{e} + \boldsymbol{c}(0)]$ and $\boldsymbol{b} = (1/\sqrt{2})[\boldsymbol{e} - \boldsymbol{c}(0)]$.

The evaluation of $G_{qq}(t)$ is accomplished by utilizing an expression analogous to eqn. (19):

$$\begin{aligned}\boldsymbol{q}^{\mathrm{T}} \cdot \boldsymbol{G}(t)\boldsymbol{q} &= \boldsymbol{q}^{\mathrm{T}} \cdot \exp(\boldsymbol{W}t)\boldsymbol{q} \\ &= \sum_{k=1}^{N} \boldsymbol{q}^{\mathrm{T}} \cdot \boldsymbol{y}_k \exp(\lambda_k t)\, \boldsymbol{y}_k^{\mathrm{T}} \cdot \boldsymbol{q} \\ &= \sum_{k=1}^{N} R_{qq}^{(k)} \exp(\lambda_k t) \end{aligned} \tag{A2}$$

As mentioned in the text, the first step in the procedure is the reduction of the diffusion operator to a symmetric, tridiagonal form; in other words, the operator is transformed from its real-space representation ($\boldsymbol{W}$) into one in which it is tridiagonal ($\boldsymbol{T}$) by the similarity transformation $\boldsymbol{T} = \boldsymbol{V}^{-1}\boldsymbol{W}\boldsymbol{V}$. The new representation is generated by constructing a sequence of orthonormal vectors (the Lanczos vectors, $\{\boldsymbol{v}_i\}$) according to the recursion formula:

$$\begin{aligned}&\beta_{i+1}\boldsymbol{v}_{i+1} = \boldsymbol{W}\boldsymbol{v}_i - \alpha_i \boldsymbol{v}_i - \beta_i \boldsymbol{v}_{i-1} \\ &\alpha_i = \boldsymbol{v}_i \cdot \boldsymbol{W}\boldsymbol{v}_i \\ &\beta_{i+1} = \| \boldsymbol{W}\boldsymbol{v}_i - \alpha_i \boldsymbol{v}_i - \beta_i \boldsymbol{v}_{i-1} \| \qquad i = 1, \ldots, L \end{aligned} \tag{A3}$$

The iterative sequence begins with $\beta_0 = 0$ and the initial vectors, $\boldsymbol{v}_1 = \boldsymbol{q}$ and $\boldsymbol{v}_0 = 0$. The α_i and β_i constitute the diagonal and off-diagonal of the $L \times L$ matrix $\boldsymbol{T}$, and the $\{\boldsymbol{v}_i\}$ form the columns of the $N \times L$ rectangular matrix $\boldsymbol{V}$. $\boldsymbol{V}^{-1}$ is equal to $\boldsymbol{V}^{\mathrm{T}}$, since the $\{\boldsymbol{v}_i\}$ are orthonormal.

In exact arithmetic, the algorithm would terminate at the Lth iteration ($\beta_{L+1} = 0$, $L \leqslant N$) with the L eigenvalues of $\boldsymbol{T}$ corresponding to the L distinct eigenvalues of $\boldsymbol{W}$ whose eigenvectors have a non-zero projection on $\boldsymbol{q}$. However, in practice this stopping criterion is no longer relevant because round-off error leads to a loss in the global orthogonality of the Lanczos vectors. Instead, the magnitude of L for the present type of problem depends on the desired accuracy. The recursion formula may be viewed as a modified Gram–Schmidt process for the generation of an orthonormal basis of the subspace spanned by the vectors $\{\boldsymbol{W}^m\boldsymbol{q}\}_{m=1}^{L}$. From this vantage point, each recursion corresponds to increasing the dimension of the underlying subspace in which the diffusion operator is approximated. Therefore, the operative criterion for terminating the algorithm is to find the value of L for which the resulting subspace contains the essential components (algebraically small eigenvalues and their residues) of $G_{qq}(t)$ to the required precision. For a given class of problems, the minimum L, $L_{\min}$, can be determined empirically by incrementing systematically the number of iterations performed for a sample system, until agreement to the desired accuracy is attained among the observables calculated for values of L larger than $L_{\min}$. Our experience and other's [14,15] have shown that depending on the problem, $L_{\min}$ can range from less than 1% of the system size for very large systems up to 70% for some moderate-size systems. $L_{\min}$'s small magnitude demonstrates that only relatively few of the eigenvectors are strongly coupled to $\boldsymbol{q}$, and the algorithm converges quickly to the space spanned by these vectors.

Despite its advantages, the Lanczos algorithm has been applied only recently on a regular basis to the solution of eigenvalue problems due to the presence of numerical instabilities. In exact arithmetic, the eigenvalues of the two matrices are identical by virtue of the similarity transformation relating $\boldsymbol{T}$ and $\boldsymbol{W}$. However, the finite precision inherent in numerical computations introduces into the spectrum of $\boldsymbol{T}$ spurious eigenvalues (eigenvalues not in $\boldsymbol{W}$'s spectrum) and multiple copies of eigenvalues of $\boldsymbol{W}$ (regardless of the eigenvalue's multiplicity). The source and behavior of this instability are now well-understood [9,10], and several procedures have been devised to either prevent the spurious eigenvalues from appearing, or to allow them to appear and then identify and remove them. Our approach, based on a procedure proposed by Cullum and Willoughby [11,12], falls into the latter category. Once $\boldsymbol{T}$ is generated, its eigenvalues and the eigenvalues of $\boldsymbol{T}'$, the matrix obtained by deleting the first row and column of $\boldsymbol{T}$, are calculated. As shown empirically by Cullum and Willoughby, the eigenvalues which appear in the spectra of both $\boldsymbol{T}$ and $\boldsymbol{T}'$ are precisely the spurious eigenvalues, and hence by comparing the two sets of eigenvalues, these unwanted eigenvalues may be identified and deleted. All but one of the multiple copies of $\boldsymbol{W}$'s eigenvalues can, of course, be trivially removed from the spectrum of $\boldsymbol{T}$. For the case where the eigenvalues of $\boldsymbol{W}$ are non-degenerate, the resulting spectrum is isomorphic to $\boldsymbol{W}$'s. If some of the eigenvalues of $\boldsymbol{W}$ are

degenerate, the method outlined here for finding the observables remains valid as shown in ref. 20.

The eigenvalues of $\boldsymbol{T}$ and $\boldsymbol{T}'$ are computed via the bisection method [21], which utilizes the Sturm-sequencing property of symmetric, tridiagonal matrices. It offers two significant computational advantages over alternative procedures. First, and most important, the procedure is readily vectorized, and consequently dramatic reductions in CPU time are realized over other tridiagonal eigenvalue routines (e.g., the QL transformation [22]), which are highly recursive and hence non-vectorizable. Prior to our adoption of the bisection method, the evaluation of the eigenvalues of $\boldsymbol{T}$ and $\boldsymbol{T}'$ dominated the computation time almost completely, whereas the portion of the program presently requires only 30–40% of the total time. A second advantage offered by the method is the selectivity in the accuracy to which different eigenvalues are found. As noted previously, only the algebraically smallest eigenvalues contribute significantly to the final result at intermediate to long times; as seen in eqn. (A4) below, the remaining eigenvalues are needed solely to find the residues of the smallest eigenvalues. We have performed numerical experiments which demonstrate that the residues of the small eigenvalues depend only weakly on those eigenvalues far removed. Consequently, the error tolerance to which the majority of the eigenvalues are found can be set to a much larger value than that required for the smaller eigenvalues, thereby permitting a further reduction in the CPU time.

The final step is the calculation of the residues $R_{qq}^{(k)}$ using the RRGM. Hence after the spurious eigenvalues and multiple copies have been purged from the spectra of $\boldsymbol{T}$ and $\boldsymbol{T}'$, the following formula is utilized to find the residue of the kth eigenvalue:

$$R_{qq}^{(k)} = \frac{\prod_{i=1}^{N-1} (\lambda_i' - \lambda_k)}{\prod_{\substack{i=1 \\ i \neq k}}^{N} (\lambda_i - \lambda_k)} \tag{A4}$$

where the λ_k and λ_k' are the eigenvalues of $\boldsymbol{T}$ and $\boldsymbol{T}'$, respectively.

The derivation of this equation is based on elementary linear algebra and the theory of Green's functions and may be found in ref. 14. We note that the ratios $(\lambda_i' - \lambda_k)/(\lambda_i - \lambda_k)$ are typically of order unity, and consequently there is no problem in implementing eqn. (A4) numerically. Also, it is clear from the expression that each residue depends on the global distribution of eigenvalues, so that the full spectra of $\boldsymbol{T}$ and $\boldsymbol{T}'$ must be found even though most modes contribute negligibly to the solution at long times. Once the eigenvalues and residues have been found, $G_{qq}(t)$ is easily assembled using eqn. (A2).

APPENDIX B. APPLICATION OF THE LANCZOS ALGORITHM AND RRGM TO NON-UNIFORM GRIDS

In digital simulations of electrochemical systems, non-uniform grids are often employed in finite difference schemes in order to reduce the computation times. For

instance, in ref. 16 an exponential space grid was utilized to obtain the long-time, quasi-steady-state behavior of a patterned array of electrodes. One important consequence of this strategy is that the transfer matrix is no longer symmetric, as is the case for uniform grids. Therefore since the formulation of the Lanczos algorithm used here is only valid for symmetric matrices, the methods described in Sect. (II) and Appendix A cannot be applied directly to $\boldsymbol{W}$. This problem can be surmounted, however, if $\boldsymbol{W}$ can be factored into a product of the form

$$\boldsymbol{W} = \boldsymbol{U}^{-1}\boldsymbol{S}\boldsymbol{U} \tag{B1}$$

where the matrix $\boldsymbol{S}$ is symmetric and the format of $\boldsymbol{U}$ is arbitrary. Given this decomposition, the Green's function can be recast as

$$\begin{aligned}\boldsymbol{G}(t) &= \exp[\boldsymbol{W}t] \\ &= \exp[\boldsymbol{U}^{-1}\boldsymbol{S}\boldsymbol{U}t] \\ &= \boldsymbol{I} + \boldsymbol{U}^{-1}\boldsymbol{S}\boldsymbol{U}t + (\tfrac{1}{2})(\boldsymbol{U}^{-1}\boldsymbol{S}\boldsymbol{U})(\boldsymbol{U}^{-1}\boldsymbol{S}\boldsymbol{U})t^2 + \ldots \\ &= \boldsymbol{U}^{-1}[\boldsymbol{I} + \boldsymbol{S}t + (\tfrac{1}{2})\boldsymbol{S}^2t^2 + \ldots]\boldsymbol{U} \\ &= \boldsymbol{U}^{-1}\exp[\boldsymbol{S}t]\boldsymbol{U}\end{aligned} \tag{B2}$$

By inserting the last expression for $\boldsymbol{G}(t)$ into eqn. (19), $G_{ei}(t)$ becomes

$$\begin{aligned}G_{ei}(t) &= \boldsymbol{e}^{\mathrm{T}} \cdot \exp[\boldsymbol{W}t]\boldsymbol{c}(0) \\ &= \boldsymbol{e}^{\mathrm{T}} \cdot \boldsymbol{U}^{-1}\exp[\boldsymbol{S}t]\boldsymbol{U}\boldsymbol{c}(0) \\ &= \boldsymbol{e}'^{\mathrm{T}} \cdot \exp[\boldsymbol{S}t]\boldsymbol{c}'(0)\end{aligned} \tag{B3}$$

with $\boldsymbol{c}'(0) = \boldsymbol{U}\boldsymbol{c}(0)$, and $\boldsymbol{e}' = \boldsymbol{U}^{-1}\boldsymbol{e}$. The procedure is now applied to this last expression for $G_{ei}(t)$ with $\boldsymbol{S}$ replacing $\boldsymbol{W}$, $\boldsymbol{e}'$ replacing $\boldsymbol{e}$, and $\boldsymbol{c}'(0)$ replacing $\boldsymbol{c}(0)$. The factorization thus enables the symmetry of $\boldsymbol{W}$ to be "transferred" to the initial concentration vector and the flux vector, so that the non-uniform space discretization falls within the domain of the Lanczos procedure.

To illustrate how the transformation in eqn. (B1) can be effected, we consider in detail the exponential grid proposed in ref. 16 and used here in the modeling of a single microband electrode. Figure 6 is a diagram of the space grid employed there, and Table 2 lists the associated simulation diffusion constants. As seen in the figure, there are N_{M} partitions in the N-direction, and J_{M} in the J-direction for a total of $N_{\mathrm{M}}J_{\mathrm{M}}$ cells; the resulting cells are labeled as indicated. The asymmetry of the transfer matrix's elements is evident from Table 2: the diffusion constants for a given cell are functions of the cell's position, so that the transfer rates into and out of a volume element across the same boundary are unequal. For example, the diffusion coefficient for transfer from cell $N_{\mathrm{M}} + 2$ to cell $2N_{\mathrm{M}} + 2([\boldsymbol{W}]_{2\mathrm{Nm}+2,\mathrm{Nm}+2})$ is $D_{\mathrm{o}}(J = 2) = D_{\mathrm{M}}\exp[-2\beta(5/4)]$, whereas for transfer in the opposite direction $([\boldsymbol{W}]_{\mathrm{Nm}+2,2\mathrm{Nm}+2})$, the diffusion coefficient is $D_{\mathrm{i}}(J = 3) = D_{\mathrm{M}}\exp[-2\beta(7/4)]$.

TABLE 2

Simulation diffusion constants [a,b]

Limit	Inner boundary	Outer boundary
$J=1$	$D_i(J)=D_M \sinh(\beta/2)\,\mathrm{cosech}(\beta/4)\exp(\beta/4)$	$D_o(J)=D_M \exp[-2\beta\{J-(3/4)\}]$
$J\geqslant 2$	$D_i(J)=D_M \exp[-2\beta\{J-(5/4)\}]$	$D_o(J)=D_M \exp[-2\beta\{J-(3/4)\}]$
$N<N1-1$	$D_i(N)=D_M \exp[-2\beta\{N1-N-(3/4)\}]$	$D_o(N)=D_M \exp[-2\beta\{N1-N-(5/4)\}]$
$N=N1-1$	$D_i(N)=D_M \exp[-2\beta\{N1-N-(3/4)\}]$	$D_o(N)=D_M$
$N1\leqslant N\leqslant N4$	$D_i(N)=D_M$	$D_o(N)=D_M$
$N=N4+1$	$D_i(N)=D_M$	$D_o(N)=D_M \exp[-2\beta\{N-N4-(3/4)\}]$
$N>N4+1$	$D_i(N)=D_M \exp[-2\beta\{N-N4-(5/4)\}]$	$D_o(N)=D_M \exp[-2\beta\{N\text{-}N4-(3/4)\}]$

[a] $D_M=(D\Delta t)/(\Delta x^2)$.

[b] $N1$ and $N4$ are the labels of the first and last cells of the region adjacent to the electrode; in Fig. 7, $N4=N1+2$.

We begin the factorization by separating $\boldsymbol{W}$ into the sum of the diagonal matrix $\boldsymbol{D}$ containing the diagonal elements of $\boldsymbol{W}$ and the matrix $\boldsymbol{O}$ of the off-diagonal entries,

$$\boldsymbol{W}=\boldsymbol{D}+\boldsymbol{O} \tag{B4}$$

The motivation for this separation is that only the off-diagonal elements of $\boldsymbol{W}$ are modified in the transformation from $\boldsymbol{W}$ to $\boldsymbol{S}$ since, as shown below, the matrix $\boldsymbol{U}$ can be chosen to be diagonal, and hence the diagonal elements of $\boldsymbol{W}$ and $\boldsymbol{S}$ are identical.

Given the labeling scheme in Fig. 6, the matrix $\boldsymbol{O}$ can be viewed as a $J_M\times J_M$ tridiagonal supermatrix with each block element of dimension $N_M\times N_M$:

$$\boldsymbol{O}=\begin{bmatrix} \boldsymbol{N} & \boldsymbol{D}_o(J=1) & \boldsymbol{0} & \cdot & \cdot & \cdot & \cdot \\ \boldsymbol{D}_i(J=2) & \boldsymbol{N} & \boldsymbol{D}_o(J=2) & \boldsymbol{0} & \cdot & \cdot & \cdot \\ \boldsymbol{0} & \boldsymbol{D}_i(J=3) & \boldsymbol{N} & \boldsymbol{D}_o(J=3) & \boldsymbol{0} & \cdot & \cdot \\ \cdot & \cdot & \cdot & \cdot & \cdot & \cdot & \cdot \\ \cdot & \cdot & \cdot & \cdot & \cdot & \boldsymbol{D}_i(J=J_M) & \boldsymbol{N} \end{bmatrix} \tag{B5}$$

The matrices $\boldsymbol{D}_i(J)$ and $\boldsymbol{D}_o(J)$ are diagonal with all elements equal to $D_i(J)$ or $D_o(J)$. The matrix $\boldsymbol{N}$ is itself tridiagonal with the superdiagonal containing the entries $[\boldsymbol{N}]_{k,k+1}=D_o(N=k)$ and the subdiagonal consisting of the elements $[\boldsymbol{N}]_{k+1,k}=D_i(N=k+1)$; from eqn. (B4) the diagonal elements of $\boldsymbol{N}$ are zero.

The factorization of $\boldsymbol{O}$ is accomplished in two independent steps: in the first step, $\boldsymbol{N}$ is decomposed into the form of eqn. (B1); we then superimpose on this the factorization of the J-blocks. This approach is feasible because the diffusion constants for a given boundary depend on only one of the two coordinates (N or J). Moreover, the procedure is completely general and can be readily extended to three-dimensional problems and other geometries for which the same condition holds.

The decomposition of $\boldsymbol{N}$ is found by assuming $\boldsymbol{N} = \boldsymbol{U}_N^{-1}\boldsymbol{S}_N\boldsymbol{U}_N$, where $\boldsymbol{U}_N$ is diagonal and $\boldsymbol{S}_N$ is symmetric and tridiagonal, and then solving recursively the resulting equations beginning with the cells next to the electrodes. The solution is

$$[\boldsymbol{U}_N]_{kk} = \begin{cases} \exp\left[\left(\frac{\beta}{2}\right)\{N1 - 1 - k\}\right] & k \leqslant N1 - 1 \\ 1 & N1 \leqslant k \leqslant N4 \\ \exp\left[\left(\frac{\beta}{2}\right)\{k - N4 - 1\}\right] & k \geqslant N4 + 1 \end{cases} \tag{B6}$$

$$[\boldsymbol{S}_N]_{k,k+1} = \begin{cases} D_{\mathrm{M}} \exp[-2\beta\{N1 - k - (3/2)\}] & k \leqslant N1 \\ D_{\mathrm{M}} & N1 - 1 \leqslant k \leqslant N4 \\ D_{\mathrm{M}} \exp[-2\beta\{k - N4 - (1/2)\}] & k \geqslant N4 + 1 \end{cases} \tag{B7}$$

The factorization of the J-blocks proceeds in an analogous fashion. Thus, writing $\boldsymbol{O}' = \boldsymbol{U}_{\mathrm{J}}^{-1}\boldsymbol{S}_{\mathrm{J}}\boldsymbol{U}_{\mathrm{J}}$ where $\boldsymbol{O}' = \boldsymbol{O} - \boldsymbol{N}$, $\boldsymbol{U}_J$ is a $J_{\mathrm{M}} \times J_{\mathrm{M}}$ block diagonal matrix (each block $N_{\mathrm{M}} \times N_{\mathrm{M}}$), and $\boldsymbol{S}_J$ is a $J_{\mathrm{M}} \times J_{\mathrm{M}}$ symmetric block tridiagonal matrix, then it is straightforward to show that the ith block of $\boldsymbol{U}_J$ is

$$[\boldsymbol{U}_J]_i = \exp[(\beta/2)(i-1)] \tag{B8}$$

and the ith superdiagonal block of S_J is

$$[\boldsymbol{S}_J]_{i,i+1} = \exp[-2\beta\{i - (1/2)\}] \tag{B9}$$

The final decomposition is found combining the two factorizations:

$$\left.\begin{array}{l} \boldsymbol{O} = \boldsymbol{U}^{-1}\boldsymbol{S}\boldsymbol{U} \\ \text{with} \\ \boldsymbol{U} = \boldsymbol{U}_J\boldsymbol{U}_N' \\ \text{and} \\ \boldsymbol{S} = \boldsymbol{S}_J + \boldsymbol{S}_N' \end{array}\right\} \tag{B10}$$

Here $\boldsymbol{U}_J$ and $\boldsymbol{S}_J$ are as defined above, and $\boldsymbol{U}_N'$ and $\boldsymbol{S}_N'$ are the $N_{\mathrm{M}}J_{\mathrm{M}} \times N_{\mathrm{M}}J_{\mathrm{M}}$ diagonal block matrices with each block equal to $\boldsymbol{U}_N$ and $\boldsymbol{S}_N$, respectively. $\boldsymbol{U}$ is clearly diagonal, and $\boldsymbol{S}$ is symmetric, so that $\boldsymbol{W}$ has been factored into the form specified in eqn. (B1), i.e.,

$$\begin{aligned} \boldsymbol{W} &= \boldsymbol{D} + \boldsymbol{O} = \boldsymbol{D} + \boldsymbol{U}^{-1}\boldsymbol{S}\boldsymbol{U} \\ &= \boldsymbol{U}^{-1}[\boldsymbol{D} + \boldsymbol{S}]\boldsymbol{U} \end{aligned} \tag{B11}$$

with $\boldsymbol{D} + \boldsymbol{S}$ symmetric.

ACKNOWLEDGEMENTS

This work was supported in part by the Robert A. Welch Foundation and an NSF Materials Research grant (DMR-8418086). The authors would like to thank the University of Texas System Center for High Performance Computing for

providing the necessary computing resources. R.A.F. would also like to thank the Alfred P. Sloan Foundation and the Camille and Henry Dreyfus Foundation for financial support.

REFERENCES

1 S.W. Feldberg in A.J. Bard (Ed.), Electroanalytical Chemistry, Vol. 3, Marcel Dekker, New York, 1969, p. 199.
2 A.J. Bard and L.R. Faulkner, Electrochemical Methods, Wiley, New York, 1980.
3 S.W. Feldberg, J. Electroanal. Chem., 127 (1981) 1.
4 R. Seeber and S. Stefani, Anal. Chem., 53 (1981) 1011.
5 L.F. Whiting and P.W. Carr, J. Electroanal. Chem., 81 (1977) 1.
6 S.W. Feldberg, J. Electroanal. Chem., 222 (1987) 101.
7 G. Strang, Linear Algebra and Its Applications, Academic Press, New York, 1976.
8 W.E. Boyce and R.C. DiPrima, Elementary Differential Equations and Boundary Values Problems, Wiley, New York, 1977.
9 C.C. Paige, J. Inst. Math. Its Appl., 10 (1972) 373.
10 C.C. Paige, J. Inst. Math. Its Appl., 18 (1976) 341.
11 J. Cullum and R.A. Willoughby, J. Comp. Phys., 44 (1981) 329.
12 J. Cullum and R.A. Willoughby, Lanczos Algorithms for Large Symmetric Eigenvalue Computations, Vol. 1, Birkhauser, Boston, MA, 1985.
13 C. Lanczos, J. Res. Natl. Bur. Stand., 45 (1950) 255.
14 A. Nauts and R.E. Wyatt, Phys. Rev. Lett., 51 (1983) 2238.
15 R.E. Wyatt in J.O. Hirschfelder, R.E. Wyatt, and R.D. Coalson (Eds.), Lasers, Molecules and Methods, Advances in Chemical Physics, Wiley, New York, to be published.
16 A.J. Bard, J.A. Crayston, G.P. Kittleson, T.V. Shea and M.S. Wrighton, Anal. Chem., 58 (1986) 2321.
17 T. Kavanaugh, M.S. Friedrichs, R.A. Friesner and A.J. Bard, in preparation.
18 W.A. Wassam, J. Chem. Phys., 82 (1985) 3371.
19 W.A. Wassam, J. Chem. Phys., 82 (1985) 3386.
20 A. Nauts, Chem. Phys. Lett., 119 (1985) 529.
21 W. Barth, R.S. Martin, and J.H. Wilkinson, Numer. Math., 9 (1967) 386.
22 C. Reinsch and F.L. Bauer, Numer. Math., 11 (1968) 264.